


Article

Effect of Ultrasonic Shot Peening on Morphology and Structure of NiCrAlYSi Coatings on Superalloys for Blade Applications

Jin Cai ^{1,*}, Hao Wu ¹  and Xihui Shi ²

¹ School of Aerospace Engineering, Shenyang Aerospace University, Shenyang 110136, China; wuhao5@stu.sau.edu.cn

² School of Mechatronics Engineering, Shenyang Aerospace University, Shenyang 110136, China; shixihui@stu.sau.edu.cn

* Correspondence: saumax@163.com

Abstract: The study evaluated and compared the surface morphology, roughness, and coating structure of ultrasonic shot peening (USP)-treated samples of the NiCrAlYSi-coated GH4169 alloy used for turbine blades and discussed the influence of blade-surface roughness and coating thickness on aerodynamic performance. The NiCrAlYSi coating was deposited on the surface of the alloy using electron beam-physical vapor deposition (EB-PVD), and the NiCrAlYSi bond coat was subsequently surface treated at Almen intensities of 0.1 A, 0.15 A, and 0.2 A by USP. The results following USP treatment indicated that the bond coat becomes denser with a smoother surface and a porosity reduction ranging from 12.5% to 50%, accompanied by localized enrichment of Cr elements near the substrate. Additionally, the study examined the influence of coating thickness and roughness on turbine blade aerodynamic performance, validating the effectiveness of USP in reducing these factors, thereby potentially enhancing the aerodynamic efficiency of coated turbine blades.

Keywords: NiCrAlYSi bond coat; ultrasonic shot peening; surface roughness; thickness; aerodynamic efficiency



Citation: Cai, J.; Wu, H.; Shi, X. Effect of Ultrasonic Shot Peening on Morphology and Structure of NiCrAlYSi Coatings on Superalloys for Blade Applications. *Coatings* **2024**, *14*, 949. <https://doi.org/10.3390/coatings14080949>

Academic Editor: Cecilia Bartuli

Received: 3 July 2024

Revised: 24 July 2024

Accepted: 26 July 2024

Published: 29 July 2024



Copyright: © 2024 by the authors. Licensee MDPI, Basel, Switzerland. This article is an open access article distributed under the terms and conditions of the Creative Commons Attribution (CC BY) license (<https://creativecommons.org/licenses/by/4.0/>).

1. Introduction

Thermal barrier coatings (TBCs) are widely employed in aerospace engines to enhance the performance and durability of high-temperature components such as turbine disks, blades, and combustion chambers. These coatings prevent high-temperature alloys from experiencing high-temperature corrosion, improve component longevity and engine efficiency, reduce fuel consumption, and extend service life [1–4]. TBCs consist of a bond coat (MCrAlX, M=Ni, Co X=Y, Si, Ta) deposited on the surface of superalloys and a ceramic top-coat. The MCrAlX bond coat provides high-temperature resistance and oxidation corrosion resistance, but its ductility and fatigue resistance are lower than those of the turbine disk superalloys. Moreover, interface defects such as pores and inclusions exist between the bond coat and superalloys [5].

The current challenge is that TBC systems have a tendency to fail by spalling or by debonding processes under cyclic high-temperature conditions. TBCs exhibit multiple failure mechanisms. The growth of the TGO between the bond coat and the top coat layers causes large residual stresses, which lead to the spallation of TBCs [6]. However, the introduction of the shot peening process may bring about a significant change to this unfavorable factor [7]. Shot peening treatment on the surface of the bond coat can introduce compressive residual stress and plastic strain, enhancing the adhesive strength, density, and oxidation resistance of the coating to the superalloys [8,9]. This leads to a good research direction, i.e., the study of the evolution of multiple microstructures of TBC systems by shot peening, including the effect on the intergranular behavior of the bonded layer, the elemental distribution along the cross-section, the microstrain along the cross-section, and so on. Karaoglanli et al. investigated the influence of shot peening treatment on CoNiCrAlY

bond coats and found that it reduced the porosity of the bond coat. Furthermore, with the increasing of Almen intensities, the growth rate of the thermally grown oxide (TGO) layer decreased, leading to an extended thermal cyclic fatigue life of the specimens [7,10]. Akebono et al. observed that the sprayed specimens with thinner coatings indicated higher fatigue strength [11]. Over the conventional shot peening technique, USP has the advantages of high processing efficiency, strong controllability of process parameters, simple operation, no pollution, and wide application. Additionally, Stoll et al. compared the effects of conventional shot peening and USP on surface roughness and fatigue life. USP, with its random distribution of spheres during the process, reduced surface roughness and shifted the crack initiation point from the surface to the subsurface, thereby extending fatigue life [12]. Existing studies have mainly focused on the surface treatment of bond coats using shot peening, and there is no literature reporting on the effects of USP on bond coating thickness, roughness, and the subsequent aerodynamic performance of turbine blades. However, it cannot be ignored that the blade coating goes through the entire aerodynamic process of the blade during its service. Apart from its inherent heat resistance, the aerodynamic performance after coupling with the blade is equally important. Therefore, this study applies USP treatments with intensities of 0.1 A, 0.15 A, and 0.2 A to NiCrAlYSi bond coats. Experimental investigations are conducted using SEM spectroscopic analysis and other instruments to analyze the morphology of the bond coat samples before and after USP treatment. Simultaneously, the aerodynamic impact of USP on the coatings of GH4169 blade alloy has been comprehensively considered and analyzed, providing a basis for the application of USP technology on coating blades.

2. Materials and Methods

The GH4169 superalloy (US Inconel 718), Fushun Special Steel Co., Ltd., Fushun, China, used in the present study is a precipitation-strengthened Ni-Fe-Cr-based deformed superalloy, and its standard chemical element composition is shown in Table 1. The GH4169 samples used in this experiment feature dimensions of 22 mm × 13 mm × 1 mm. The bond coat selected is NiCrAlYSi, and the material's chemical composition is shown in Table 1. The NiCrAlYSi bond coat is deposited on the sample surface using EB-PVD(EB-PVD-100), Beijing Aerospace Xingda Machinery Manufacturing Co., Ltd., Beijing, China, with a thickness of approximately 40 μm. The control of the right time and power stability is the guarantee of getting a quality coating. In this EB-PVD process, the electron beam power is 800 VA, with a deposition at 700 °C substrate temperature for 2 h. Prior to deposition, the sample surface is subjected to sandblasting treatment, followed by rust removal and polishing of the base alloy surface. Subsequently, residual particles, oil residues, and other contaminants on the sample surface are removed using deionized water and ethanol solution.

Table 1. Chemical composition of GH4169 alloy and NiCrAlYSi bond coating (at. %).

Material	Fe	Ni	Co	Mo	Al	Ti	Cr	C	Y	Si
GH4169	Bal.	50–55.0	1.0	2.8–3.3	0.3–0.7	0.8–1.2	17.0–21.0	0.08	-	-
NiCrAlYSi	0.3	Bal.	-	-	8.0–10.0	-	18.0–22.0	0.05	0.5–0.8	0.5–0.8

During the USP process, ultrasonic waves are generated using a piezoelectric excitation oscillator and transmitted by an amplifier on the ultrasonic generator. With the chamber in a completely sealed state, the spheres repeatedly move between the component, chamber sidewalls, and chamber roof, achieving random impacts on the sample surface, as shown in Figure 1. The spheres are made of GCr15 bearing steel, with a diameter of 2.5 mm and the number of 500. The USP durations for the samples were 360 s, 480 s, and 960 s, corresponding to the Almen intensity of 0.1 A, 0.15 A, and 0.2 A, respectively. To observe the cross-sectional organization, specimens underwent corrosion treatment using Kroll reagent. The microstructure of the samples was analyzed using a SEM (Magellan 400 FEI), FEI, Hillsboro, OR, USA, and elemental scanning analysis of characteristic regions was conducted using an EDS, FEI, Hillsboro, OR, USA. Roughness measurements were carried

out on the surface of all samples using a contact profilometer (Mar Surf GD 25, Mahr, Göttingen, Germany). For the roughness measurements, the contact needle measures 5.5 mm at a speed of 0.4 mm/s along a direction parallel to the axial direction of the sample. To improve the accuracy of the measurements, each sample was measured repeatedly three times and the average of three measurements was taken.

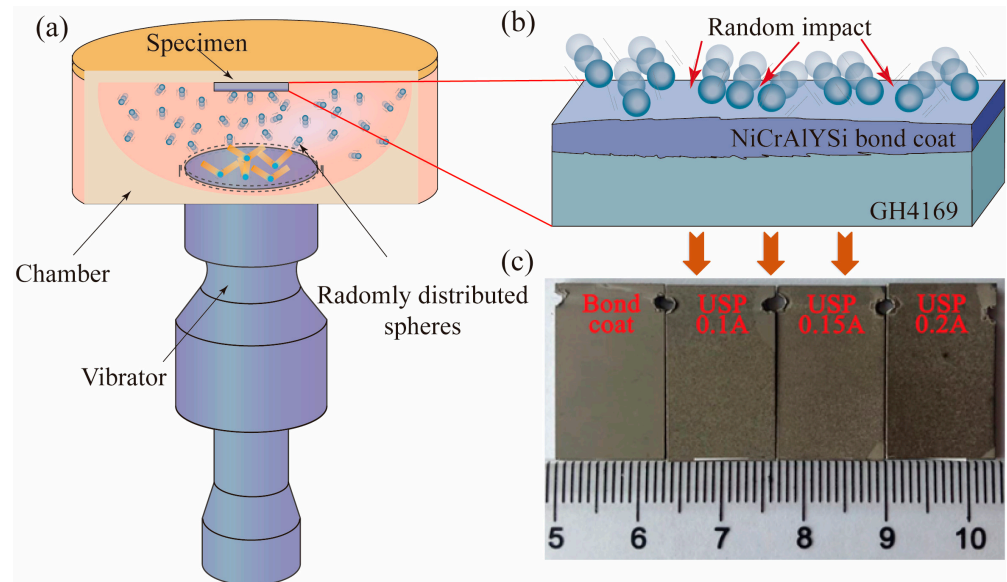


Figure 1. Schematic diagram of USP: (a) USP device, (b) dynamic process of spheres impact, (c) macroscopic morphology of the sample.

3. Results and Discussion

3.1. Morphology of NiCrAlYSi Bond Coats

Figure 1 illustrates the surface morphology of the bond coat samples before and after shot peening treatment. By using electron beam heating or vaporization, NiCrAlYSi material is deposited onto the substrate in atomic or molecular form, forming the bond coat. During the particle deposition process, interactions occur, resulting in grooves, voids, and microcracks [13]. From the macroscopic morphology, it can be observed that the surface brightness of the bond coat is reduced after USP treatment, and the particles on the coating surface are more evenly distributed.

Figure 2 displays the microstructure of the bond coat and the USP samples. The bond coat surface exhibits lump-like protrusions, loose particles, and a small number of incompletely melted particles. Compared to the GH4169 substrate, the NiCrAlYSi bond coat appears dark gray, with a distinct GH4169/NiCrAlYSi interface that exhibits noticeable cracks and porosity defects. The distribution of the bond coat's internal structure is uneven, with dark and bright phases corresponding to the rich β -Al phase and γ -Ni phase, respectively [14]. After USP treatment, the bond coat surface becomes smoother, denser, and with a lower content of microcracks. From the cross-section morphology of the samples, it can be observed that the bond coat thickness decreases and the crack content in the GH4169/NiCrAlYSi interface region decreases. The previous literature [15] has also reported a reduction in the porosity of the bond coat due to shot peening treatment, with a decreasing trend in porosity with increasing intensity.

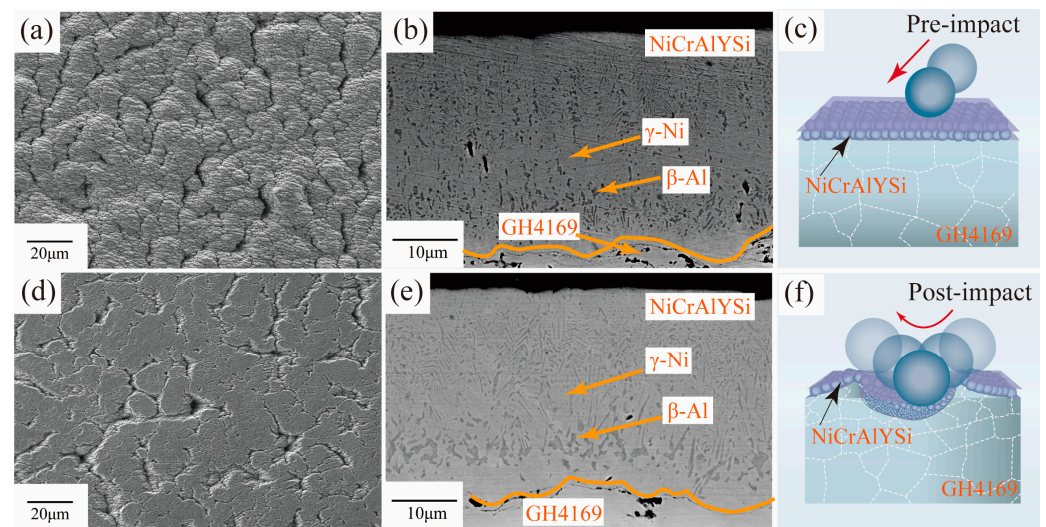


Figure 2. SEM morphology of the samples. (a) Surface of the bond coats, (b) cross-section of the bond coats, (c) schematic diagram before sphere impact coats, (d) surface of the USP sample, (e) cross-section of the USP sample, (f) schematic diagram after sphere impact coats.

3.2. Effect of USP on Surface Roughness of the Bond Coats

In this study, the measured arithmetic mean deviation R_a values and the microscopic unevenness ten-point height R_z values were used to characterize the changes in surface roughness of the coated specimens before and after USP treatments (reference Table 2 and Figure 3). As shown in Figure 3b, the surface of the coated specimens without USP resulted in larger values of R_a and R_z compared to the treated specimens, with values of R_a and R_z being 58.2% and 78.6% higher, respectively, under the intensity of 0.1 A; similar results had been obtained in previous studies [7,15]. The main reason for this phenomenon is that the random impact effect of shots introduced by USP on the surface weakens the unevenness of the coating surface caused by the coating particles, reduces the average profile roughness, weakens the protrusions and depressions on the coating surface, and makes the coating tend to be flat. According to the research of Suder et al. (see Figure 6 in [16]), the roughness of the coating surface will affect the aerodynamic efficiency by about 5%. For the USP-treated samples, within a certain range, an increase in peening duration results in an increase in the number of pits and exacerbation of surface protrusions and pits, ultimately leading to an increase in surface roughness. R_a reaches $0.79 \mu\text{m}$ when the USP intensity is 0.1 A. When the USP intensity increases to 0.2 A, the surface roughness only increases to approximately $0.85 \mu\text{m}$, mainly since increasing the USP intensity after the coverage is more significant than 100% has little effect on the surface morphology [17].

Table 2. Surface roughness of Coated and Coated +USP-treated specimens.

Treatment Process	Roughness (μm)	Average	Standard Deviation
Coated	R_a	1.25	0.045
	R_z	6.52	0.363
Coated + USP 0.1 A	R_a	0.79	0.023
	R_z	3.65	0.152
Coated + USP 0.15 A	R_a	0.83	0.027
	R_z	3.83	0.173
Coated + USP 0.2 A	R_a	0.85	0.032
	R_z	4.24	0.182

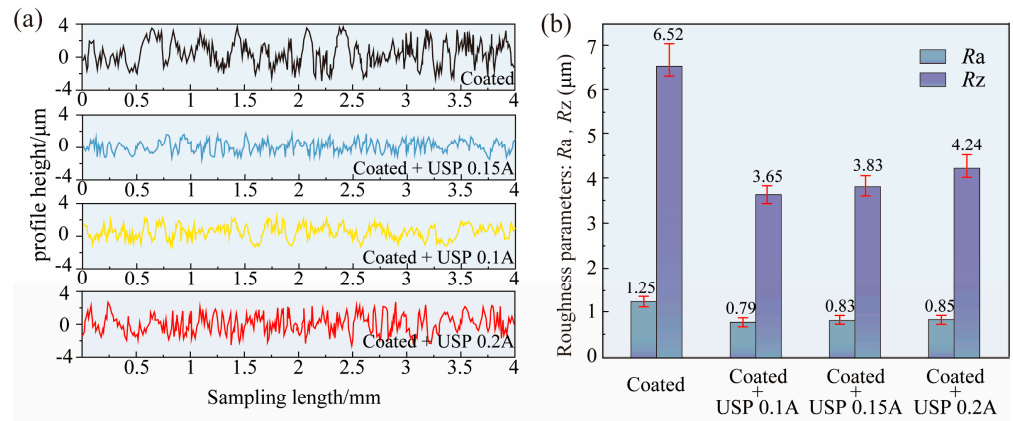


Figure 3. Surface roughness of GH4169 alloy with different Almen intensities: (a) 2D roughness profiles; (b) surface roughness.

3.3. Elemental Distribution and Coating Thickness of NiCrAlYSi Bond Coats

Figure 4 presents the line scan analysis results of the samples at different intensities. Line scans were performed along the PQ and P1Q1 lines to analyze the composition. In the bond coat region near the substrate, enrichment peaks of Cr and O elements are observed. Quantitative analysis of the M and N points in Figure 4b yields the results shown in Table 3. This indicates that, in addition to Al-containing oxides, the bond coat also contains a significant amount of Cr oxides. This is mainly due to the chemical reactions between Al, Cr, and O elements during USP forming a protective layer that prevents further diffusion of O elements into the substrate [18]. As shown in Figure 4d,e, at intensities of 0.1 A and 0.15 A, the content of Cr on the surface area accounts for 13% and 22% of the total elemental content, respectively. This suggests the potential introduction of Cr elements from the GCr15 spheres to the surface of the bond coat samples, which can be further analyzed and verified through comparative experiments using ceramic spheres (ZrO₂, Si₃N₄) or glass spheres. As shown in Figure 4a, during the USP process, the kinetic energy of the spheres is converted into internal stress, inducing dislocation motion and the formation of small-angle grain boundaries and subgrain boundaries within the bond coat, thereby increasing the diffusion pathway for Cr elements [19]. With the Almen intensity increasing, Cr elements within the bond coat migrate towards the surface, and chromium is known to enhance the wear resistance and antioxidative properties of the coated sample surface [20–24].

Table 3. Chemical element composition in the bond coat (at.%).

Point	O	Al	Cr	Ni
M	28.68	18.72	34.44	18.16
N	12.93	12.93	27.82	29.03

Figure 5 illustrates the distribution of O, Al, Cr, and Ni elements on the cross-section of the samples at different Almen intensities. During the USP process, localized high temperatures on the substrate surface lead to melting, facilitating the embedding of the NiCrAlYSi bond coat into the substrate, resulting in an uneven bond coat–substrate interface. Al, Cr, and Ni elements exhibit significant elemental segregation in the interface region between the bond coat and the substrate, with notable compositional differences. At the GH4169/NiCrAlYSi interface region, there are Al₂O₃ inclusions, primarily due to the presence of a small amount of residual sand particles on the substrate surface from the sandblasting treatment prior to bond coat deposition, as indicated by the dashed circular region in Figure 5b. Surface scanning analysis provides a visual observation of the coating thickness and the surface distribution of various elements. The results demonstrate a significant decrease in bond coat thickness with the increasing of the Almen intensities, as

indicated by d_1 and d_2 in Figure 5, which may affect further fatigue crack propagation behavior. With the increase in Almen intensity, the decrease in bond coat thickness suppresses fatigue crack propagation behavior by increasing surface residual stress and enhancing the material's surface strengthening effect. Reducing the thickness of the bond coat can lead to higher residual stress, which helps to impede crack propagation. Faksa et al. found that the cracks that were initially open after CVD coating were closed after shot peening. Well-chosen impact energies closed cracks firmly without damaging the inserts [25].

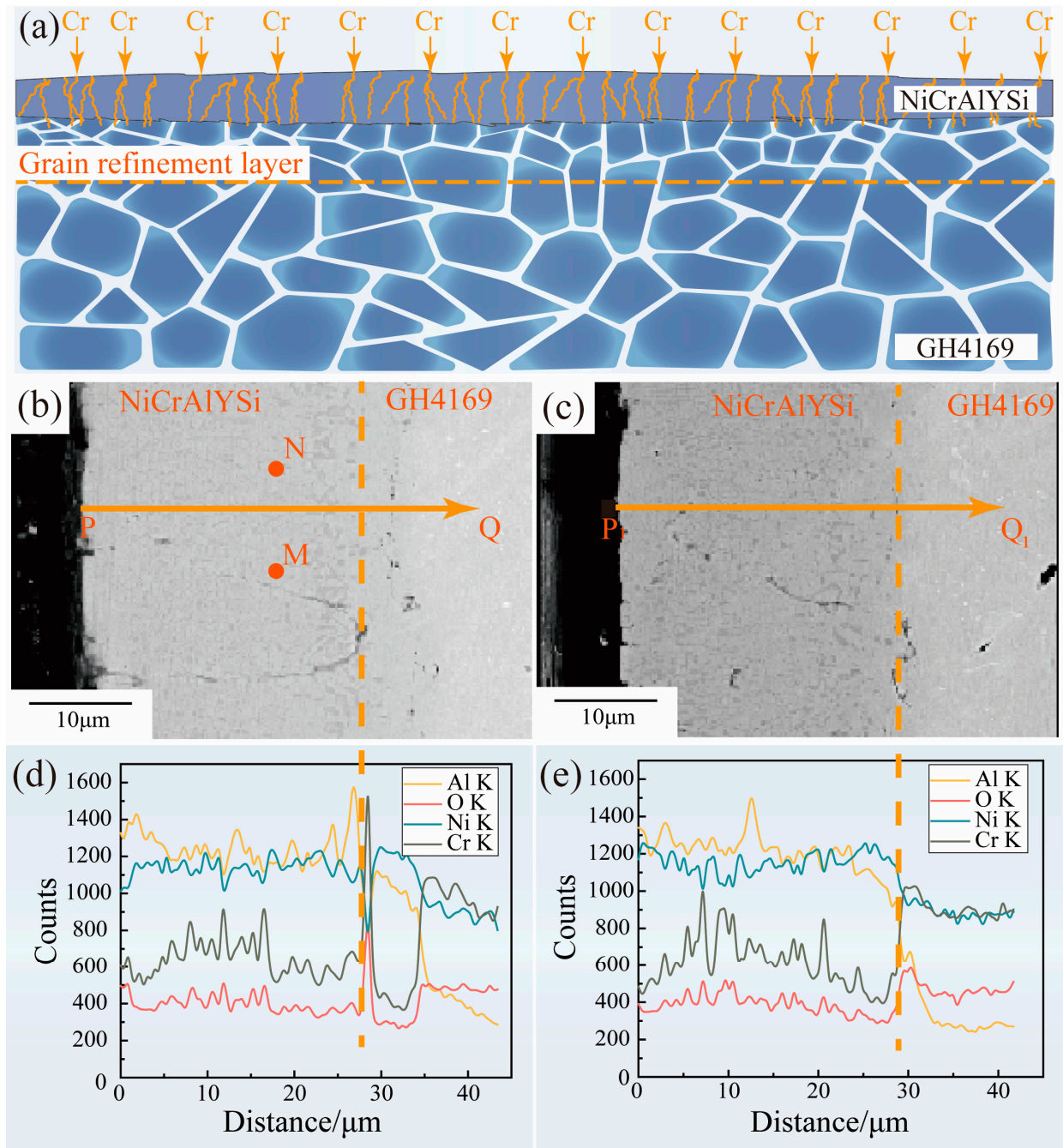


Figure 4. Line scanning analysis of samples after USP with different intensities. (a) Element penetration diagram, (b,d) scanning results by intensity of 0.1 A, (c,e) scanning results by intensity of 0.15 A.

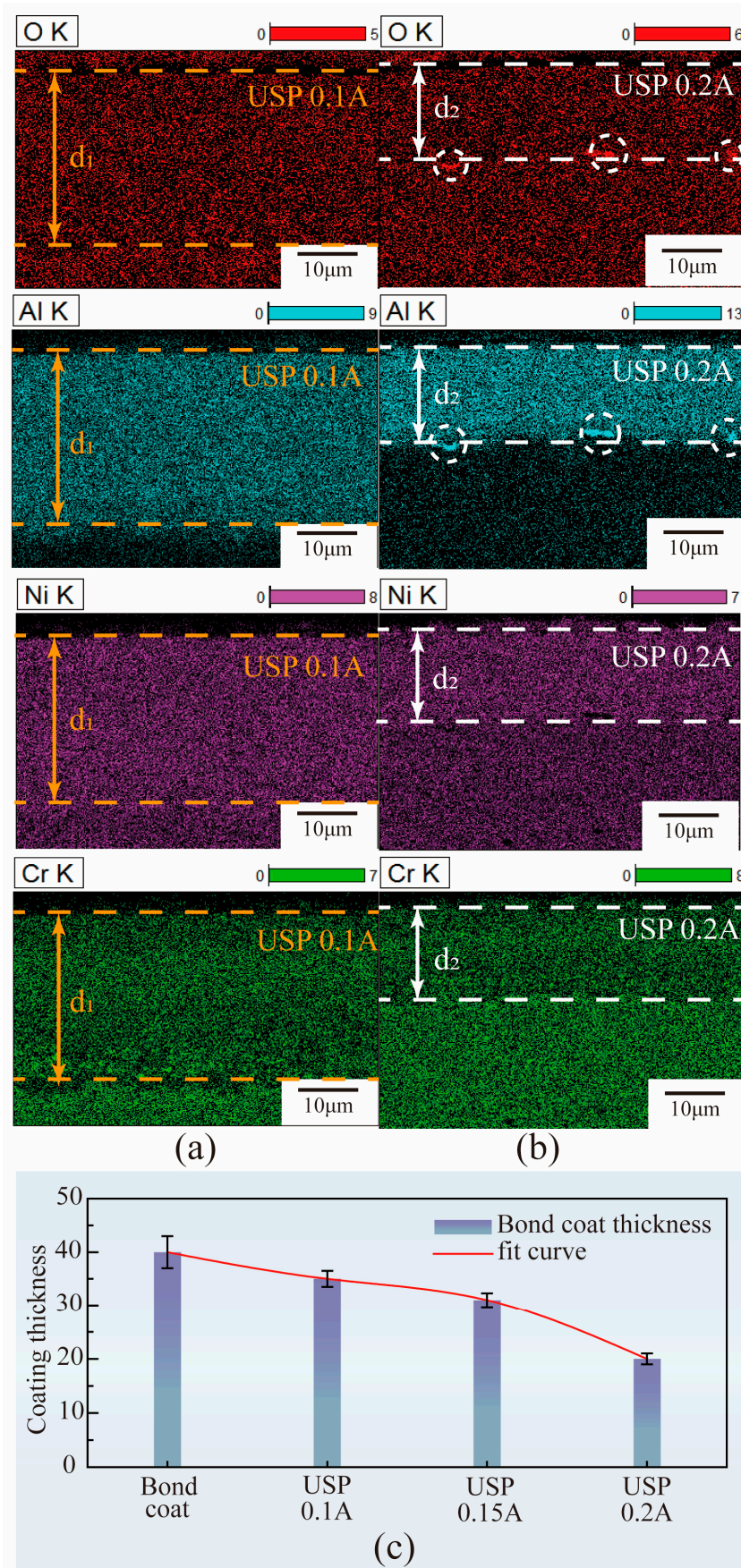


Figure 5. Section distribution of O, Al, Cr, and Ni elements after USP with intensities (a) 0.1 A, (b) 0.2 A, and (c) the effect of different intensities on thickness.

The aerodynamic efficiency of the blade is highly sensitive to the thickness and roughness of the coating, such that any reduction in the coating thickness can potentially affect its aerodynamic performance to some extent (reference Figure 6). Suder et al. observed that coating both surfaces increased the leading-edge thickness by 10% at the hub and 20% at the tip. Application of this coating results in a loss in efficiency of six points and a 9% reduction in the pressure ratio across the rotor at an operating condition near the design point [16]. Figure 5c demonstrates the impact of different intensities on the bond coat thickness. The bond coat thickness in the non-peened sample is 40 μm . In the USP samples, the bond coat thickness at intensities of 0.1 A, 0.15 A, and 0.2 A is reduced to 35 μm , 31 μm , and 20 μm , respectively, with a reduction range of 12.5% to 50%. As the intensity of USP treatment increases, the bond coat thickness exhibits a decreasing trend, resulting in a greater reduction in thickness compared to the non-peened sample.

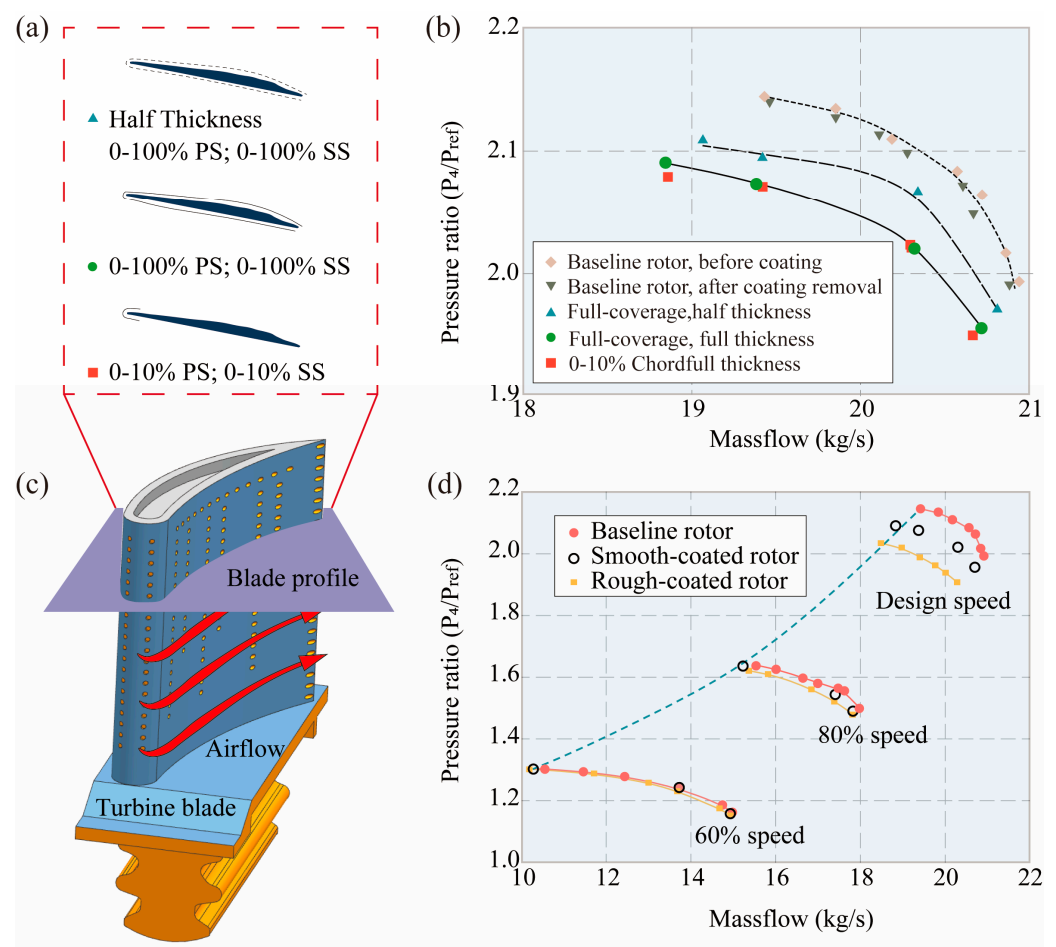


Figure 6. Effects of turbine blade coats thickness and roughness on aerodynamic efficiency. (a) Airfoil section diagram, including half full coverage thickness, full coverage normal thickness, 10% coverage; SS: Denotes suction surface, PS: Denotes pressure surface. (b) Effect of thickness, P_4 : total pressure, P_{ref} : standard-day total pressure. (c) Turbine blade diagram. (d) Effect of roughness [16].

Consequently, USP can not only reduce the thickness and roughness of the coated samples but also control the surface morphology changes through the adjustment of its own parameters. However, such changes exhibit minor differences under macroscopic surface conditions, and further research is needed to investigate their impact on microcracks and fatigue properties. In the current experimental process, we employed USP treatment on the samples to investigate its impact on the thickness and roughness of the existing coatings. This approach serves as an alternative equivalent to the application on turbine blades, where the coated surfaces often exhibit uneven characteristics. The presence of

small protrusions and gaps on the surface affects the flow trajectory of the airflow over the blade surface, akin to the generation of multiple micro-vortices at the gaps on the blade surface [26]. This, in turn, leads to the introduction of a certain level of resistance, as illustrated in Figure 7b.

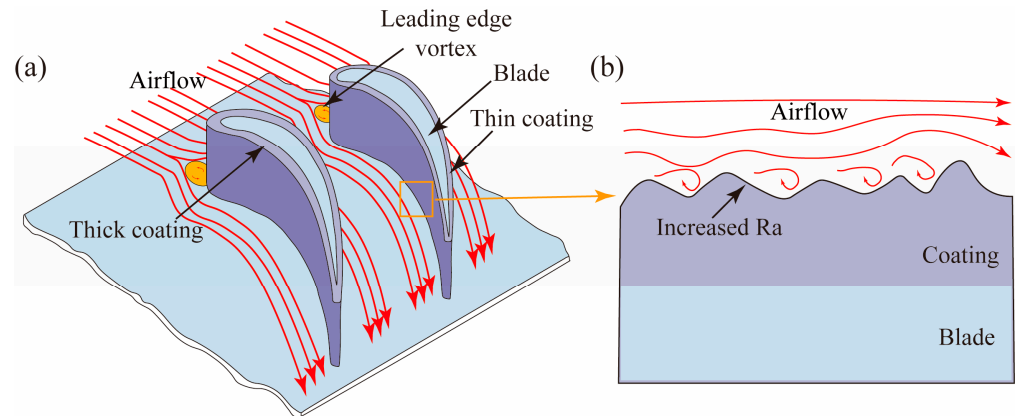


Figure 7. Schematic diagram of aerodynamic process of turbine blade. (a) Air flows through the turbine blades. (b) Air flows through the rough surface of the turbine blade.

On the other hand, the impact of coating thickness is analogous to the process of “flow around a cylinder” in the context of airfoil shapes [27,28]. In this process, resistance zones appear at the front and rear ends of the cylinder, and the larger the size of the cylinder, the greater the resistance. However, unlike cylinders, airfoils exhibit a characteristic shape with a thicker leading edge and a thinner trailing edge, which reduces the area of the flow resistance zone and enhances aerodynamic efficiency. The thinning of the airfoil coating caused by USP facilitates this enhancement of aerodynamic efficiency resulting from thickness changes. Although this impact is less than 5% [16], it is sufficient to garner attention in engineering applications (as shown in Figure 7a). To this end, further research will be conducted to explore the impact of USP on the aerodynamic efficiency of actual turbine blades. Naturally, this endeavor necessitates the development of more sophisticated USP equipment and the employment of more precise aerodynamic calculation methodologies.

4. Conclusions

In this study, the influence of USP on the surface morphology, roughness, and element distribution of the coated GH4169 superalloy for turbine blades was analyzed. Furthermore, the effects of blade coating thickness and roughness on aerodynamic performance were discussed. The following conclusions were drawn:

- (1) In terms of macroscopic morphology, the surface brightness of the bond coat is reduced after USP treatment, and the coating surface exhibits a more uniform particle distribution. At the microscopic morphology level, the bond coat becomes denser, with a reduced porosity and a smoother surface after USP treatment, leading to better adhesion between the bond coat and the substrate. Meanwhile, as the intensity increases, the bond coat thickness decreases, even with a reduction range of 12.5% to 50%.
- (2) After USP treatment, the surface of the bond coat incorporates Cr elements from the GCr15 spheres and the surface Cr content increases with increasing intensity. At an intensity of 0.1 A, localized enrichment of Cr elements is observed in the bond coat region near the substrate, indicating the presence of Cr oxides in addition to Al oxides within the bond coat after USP treatment, hindering the diffusion of O elements into the substrate.
- (3) The impact of coating thickness and roughness on the aerodynamic performance of turbine blades is discussed. USP has been well validated in reducing coating thickness and roughness, which is expected to significantly enhance the aerodynamic efficiency

of coated turbine blades, as evidenced by the previous literature. However, it is regrettable that the present study did not conduct experimental or computational analysis on the effects of roughness and thickness on blade aerodynamic performance but only provided a discussion and analysis. This will be the focus of further research aiming to establish a complex setup tailored for USP application on turbine blades. Through computational and experimental methods, the influence of coated blade surface variations on aerodynamic performance will be analyzed.

Author Contributions: Conceptualization, J.C.; Methodology, H.W.; Software, X.S. All authors have read and agreed to the published version of the manuscript.

Funding: This research did not receive any specific grant from funding agencies in the public, commercial, or not-for-profit sectors.

Data Availability Statement: The authors declare that the data supporting the findings of this study are available within the paper, and, should any raw data files be needed in another format, they are available from the corresponding author upon reasonable request.

Conflicts of Interest: The authors declare that they have no known competing financial interests or personal relationships that could have appeared to influence the work reported in this paper.

References

1. Bose, S. *High Temperature Coatings*; Butterworth-Heinemann: Oxford, UK, 2017.
2. Padture, N.P.; Gell, M.; Jordan, E.H. Thermal barrier coatings for gas-turbine engine applications. *Science* **2002**, *296*, 280–284. [[CrossRef](#)] [[PubMed](#)]
3. Aktaa, J.; Sfar, K.; Munz, D. Assessment of TBC systems failure mechanisms using a fracture mechanics approach. *Acta Mater.* **2005**, *53*, 4399–4413. [[CrossRef](#)]
4. Chen, L.; Meng, G.H.; Li, C.J.; Yang, G.J. Critical scale grain size for optimal lifetime of TBCs. *J. Mater. Sci. Technol.* **2022**, *115*, 241–250. [[CrossRef](#)]
5. Nowak, W.; Naumenko, D.; Mor, G.; Mor, F.; Mack, D.E.; Vassen, R.; Quadackers, W.J. Effect of processing parameters on MCrAlY bondcoat roughness and lifetime of APS–TBC systems. *Surf. Coat. Technol.* **2014**, *260*, 82–89. [[CrossRef](#)]
6. Giolli, C.; Scrivani, A.; Rizzi, G.; Borgioli, F.; Bolelli, G.; Lusvardi, L. Failure mechanism for thermal fatigue of thermal barrier coating systems. *J. Therm. Spray Technol.* **2009**, *18*, 223–230. [[CrossRef](#)]
7. Karaoglanli, A.C.; Doleker, K.M.; Demirel, B.; Turk, A.; Varol, R. Effect of shot peening on the oxidation behavior of thermal barrier coatings. *Appl. Surf. Sci.* **2015**, *354*, 314–322. [[CrossRef](#)]
8. Itoh, Y.; Saitoh, M.; Takaki, K.; Fujiyama, K. Effect of high-temperature protective coatings on fatigue lives of nickel-based superalloys. *Fatigue Fract. Eng. Mater. Struct.* **2001**, *24*, 843–854. [[CrossRef](#)]
9. Gabb, T.P.; Rogers, R.B.; Nesbitt, J.A.; Puleo, B.J.; Miller, R.A.; Telesman, I.; Locci, I.E. Powder Metallurgy Disk Superalloy. 2017. Available online: <https://ntrs.nasa.gov/citations/20170005889> (accessed on 2 July 2024).
10. Kumar, S.; Chattopadhyay, K.; Singh, V. Effect of ultrasonic shot peening on LCF behavior of the Ti–6Al–4V alloy. *J. Alloys Compd.* **2017**, *724*, 187–197. [[CrossRef](#)]
11. Akebono, H.; Komotori, J.; Suzuki, H. The effect of coating thickness on fatigue properties of steel thermally sprayed with Ni-based self-fluxing alloy. *Int. J. Mod. Phys. B* **2006**, *20*, 3599–3604. [[CrossRef](#)]
12. Stoll, I.; Helm, D.; Polanetzki, H.; Wagner, L. Ultrasonic Shot Peening (USP) on Ti-6Al-4V and Ti-6Al-2Sn-4Zr-6Mo Aero Engine Components. ICSP-11 2011. Available online: <https://www.shotpeener.com/library/pdf/2011062.pdf> (accessed on 2 July 2024).
13. Karaoglanli, A.C.; Altuncu, E.; Ozdemir, I.; Turk, A.; Ustel, F. Structure and durability evaluation of YSZ+ Al₂O₃ composite TBCs with APS and HVOF bond coats under thermal cycling conditions. *Surf. Coat. Technol.* **2011**, *205*, S369–S373. [[CrossRef](#)]
14. Sohn, Y.H.; Kim, J.H.; Jordan, E.H.; Gell, M. Thermal cycling of EB-PVD/MCrAlY thermal barrier coatings: I. Microstructural development and spallation mechanisms. *Surf. Coat. Technol.* **2001**, *146*, 70–78. [[CrossRef](#)]
15. Moridi, A.; Hassani-Gangaraj, S.M.; Vezzú, S.; Trško, L.; Guagliano, M. Fatigue behavior of cold spray coatings: The effect of conventional and severe shot peening as pre-/post-treatment. *Surf. Coat. Technol.* **2015**, *283*, 247–254. [[CrossRef](#)]
16. Suder, K.L.; Chima, R.V.; Strazisar, A.J.; Roberts, W.B. The effect of adding roughness and thickness to a transonic axial compressor rotor. *J. Turbomach.* **1995**, *117*, 491–505. [[CrossRef](#)]
17. Si, C.; Sun, W.; Tian, Y.; Cai, J. Cavitation erosion resistance enhancement of the surface modified 2024T351 Al alloy by ultrasonic shot peening. *Surf. Coat. Technol.* **2023**, *452*, 129122. [[CrossRef](#)]
18. Curry, N.; Tang, Z.; Markocsan, N.; Nylén, P. Influence of bond coat surface roughness on the structure of axial suspension plasma spray thermal barrier coatings—Thermal and lifetime performance. *Surf. Coat. Technol.* **2015**, *268*, 15–23. [[CrossRef](#)]
19. Voorwald, H.J.C.; Padilha, R.; Costa, M.Y.P.; Pigatin, W.L.; Cioffi, M.O.H. Effect of electroless nickel interlayer on the fatigue strength of chromium electroplated AISI 4340 steel. *Int. J. Fatigue* **2007**, *29*, 695–704. [[CrossRef](#)]

20. Zhang, X.H.; Liu, D.X.; Tan, H.B.; Wang, X.F. Effect of TiN/Ti composite coating and shot peening on fretting fatigue behavior of TC17 alloy at 350 C. *Surf. Coat. Technol.* **2009**, *203*, 2315–2321. [[CrossRef](#)]
21. Pawlak, W.; Kubiak, K.J.; Wendler, B.G.; Mathia, T.G. Wear resistant multilayer nanocomposite WC_{1-x}/C coating on Ti–6Al–4V titanium alloy. *Tribol. Int.* **2015**, *82*, 400–406. [[CrossRef](#)]
22. Richard, C.; Kowandy, C.; Landoulsi, J.; Geetha, M.; Ramasawmy, H. Corrosion and wear behavior of thermally sprayed nano ceramic coatings on commercially pure Titanium and Ti–13Nb–13Zr substrates. *Int. J. Refract. Met. Hard Mater.* **2010**, *28*, 115–123. [[CrossRef](#)]
23. Tan, L.; Ren, X.; Sridharan, K.; Allen, T.R. Effect of shot-peening on the oxidation of alloy 800H exposed to supercritical water and cyclic oxidation. *Corros. Sci.* **2008**, *50*, 2040–2046. [[CrossRef](#)]
24. Ni, L.-Y.; Wu, Z.-L.; Zhou, C.-G. Effects of surface modification on isothermal oxidation behavior of HVOF-sprayed NiCrAlY coatings. *Prog. Nat. Sci. Mater. Int.* **2011**, *21*, 173–179. [[CrossRef](#)]
25. Faksa, L.; Daves, W.; Ecker, W.; Klünsner, T.; Tkadletz, M.; Czettl, C. Effect of shot peening on residual stresses and crack closure in CVD coated hard metal cutting inserts. *Int. J. Refract. Met. Hard Mater.* **2019**, *82*, 174–182. [[CrossRef](#)]
26. Wu, Y.; Christensen, K.T. Spatial structure of a turbulent boundary layer with irregular surface roughness. *J. Fluid Mech.* **2010**, *655*, 380–418. [[CrossRef](#)]
27. Acharya, S.; Mahmood, G. Turbine blade aerodynamics. *Gas Turbine Handb.* **2006**, *1*, 364–380.
28. Hamakhan, I.; Korakianitis, T. Aerodynamic performance effects of leading-edge geometry in gas-turbine blades. *Appl. Energy* **2010**, *87*, 1591–1601. [[CrossRef](#)]

Disclaimer/Publisher’s Note: The statements, opinions and data contained in all publications are solely those of the individual author(s) and contributor(s) and not of MDPI and/or the editor(s). MDPI and/or the editor(s) disclaim responsibility for any injury to people or property resulting from any ideas, methods, instructions or products referred to in the content.